Brain Pathology ISSN 1015-6305

RESEARCH ARTICLE

Deletion of Beta-2-Microglobulin Ameliorates Spinal Cord Lesion Load and Promotes Recovery of Brainstem NAA Levels in a Murine Model of Multiple Sclerosis

Aleksandar Denic[1]; Istvan Pirko[1]; Bharath Wootla[1]; Allan Bieber[1]; Slobodan Macura[2]; Moses Rodriguez[1,3]

Departments of [1] Neurology, [2] Biochemistry and [3] Immunology, Mayo Clinic, Rochester, MN.

Keywords
axonal loss, beta-2-microglobulin, demyelination, N-acetyl aspartate (NAA), Theiler's murine encephalomyelitis virus (TMEV).

Corresponding author:
Moses Rodriguez, MD, Department of Neurology, Mayo Clinic, 200 First Street SW, Rochester, MN 55905 (E-mail: *rodriguez.moses@mayo.edu*)

Received 7 November 2011
Accepted 25 January 2012
Published Online Article Accepted 15 February 2012

doi:10.1111/j.1750-3639.2012.00576.x

Abstract

We used genetic deletion of β2-microglobulin to study the influence of $CD8^+$ T cells on spinal cord demyelination, remyelination, axonal loss and brainstem N-acetyl aspartate levels during the acute and chronic phases of Theiler's murine encephalomyelitis virus (TMEV) infection. We used $\beta2m^{-/-}$ and $\beta2m^{+/+}$ B10.Q mice (of H-2^q background) normally susceptible to TMEV-induced demyelination. Over the disease course, $\beta2m^{+/+}$ mice had increasing levels of demyelination and minimal late-onset remyelination. In contrast, $\beta2m^{-/-}$ mice had steady levels of demyelination from 45–390 dpi and remyelination was extensive and more complete. Early in the disease, brainstem NAA levels drop in both strains, but accordingly with remyelination and axonal preservation, NAA recover in $\beta2m^{-/-}$ mice despite equivalent brainstem pathology. At 270 dpi, $\beta2m^{+/+}$ mice had significantly fewer spinal cord axons than $\beta2m^{-/-}$ mice (up to 28% less). In addition, $\beta2m^{+/+}$ mice lost axons of all calibers, whereas $\beta2m^{-/-}$ mice had a modest loss of only medium- and large-caliber axons. This study further supports the hypothesis that $CD8^+$ T cells are involved in demyelination, and axonal loss following Theiler's virus-induced demyelination.

INTRODUCTION

Multiple sclerosis (MS) is a chronic inflammatory disease of the central nervous system (CNS) with varied clinical presentations and heterogeneous histopathological features. The disease leads to demyelination and axonal damage, resulting in permanent neurological deficits. The etiology of MS remains elusive. For many years, research in MS has been focused on $CD4^+$ T cells, mostly because experimental autoimmune encephalomyelitis (EAE), the most commonly studied mouse model of MS, is driven by this T-cell subtype. Only during the last decade, $CD8^+$ T cells are being more extensively studied and implicated as major mediators of immune attack and progression in human MS (14, 15). Pathological studies demonstrated that this T-cell subset outnumbers $CD4^+$ T cells (50:1), predominates in all stages of lesion formation (7, 16, 20) and that they are in close association with demyelinated axons and oligodendrocytes (36). In addition, clonal expansion of $CD8^+$ T cells rather than $CD4^+$ T cells is more frequently observed in MS lesions (14, 15, 21). Using single-cell PCR, clonal expansion of $CD8^+$ T cells has been demonstrated in active MS lesions (1), as well as in cerebrospinal fluid (CSF) and blood (48). Even though epitopes that are recognized by these $CD8^+$ T cells are unknown, the presence of clonal expansion implies unique specificity for particular epitopes. Furthermore, a recent clinical study demonstrated a CSF enrichment of highly differentiated $CD8^+$ T cells rather than $CD4^+$ T cells in early MS (19). Axonal damage correlated with the number of $CD8^+$ T cells (6), and acute MS lesions with the most severe axonal damage correlated with infiltrating $CD8^+$ T cells (23). Finally, a close contact of $CD8^+$ T cells and demyelinated axons in MS brains was observed (36) with granzyme B-positive granules polarized toward axons, indicative of a direct cytotoxic attack.

Previous studies have focused on determining the role of $CD8^+$ T cells in demyelination and axonal injury. Freshly activated myelin-specific $CD8^+$ T cell lines, when adoptively transferred, were able to induce CNS pathology in mice (13, 18, 50). We recently demonstrated that $CD8^+$ T cells are necessary and sufficient to directly injure demyelinated axons in virus-induced demyelinating disease in mice. Transfer of $CD8^+$ spinal cord-infiltrating T cells rapidly and irreversibly impaired motor function, disrupted spinal cord motor conduction and reduced the number of medium- and large-caliber spinal axons in profoundly demyelinated but functionally preserved perforin-deficient host mice (11). Further insights into the role of T cells were obtained from clinical trials with various monoclonal antibodies. Whereas anti-CD4 monoclonal antibody cM-T412 failed to provide a therapeutic effect (53), alemtuzumab, an anti-CD52 monoclonal antibody that depletes both $CD4^+$ and $CD8^+$ T cells, showed significant reduction in relapses and new lesions (9). In addition, prevention of both $CD4^+$ and $CD8^+$ T cells migration into the CNS with a natalizumab, the first α4 integrin inhibitor, had beneficial effects in MS patients (38).

A β_2-microglobulin deficient mouse ($\beta_2m^{-/-}$) proved useful in studying the role of $CD8^+$ T cells in Theiler's murine

encephalomyelitis virus (TMEV)-induced demyelinating disease in mice (3, 42, 52). Generally, β_2m-deficient mice develop normally; however, because of limited amounts of major histocompatibility complex (MHC) class I molecules on cell surface, $CD8^+$ T cells are virtually absent in these mice (22). This feature makes $\beta_2m^{-/-}$ mice very suitable for testing the roles of $CD8^+$ T cells in the TMEV model of MS. Class I-restricted $CD8^+$ T cells were implicated as effectors of resistance when targeted disruption of β_2m resulted in TMEV susceptibility in animals with resistant (H-2^b) genetic background (45). Interestingly, although β_2m-deficient mice developed demyelination comparable to normally susceptible control mice, they exhibited normal motor function and hind limb motor-evoked potentials (42, 45). This suggests that despite demyelination, absence of $CD8^+$ T cells allows preservation of axons along with the motor function. In addition, retrograde-labeling experiments showed significant decrease in axonal transport in demyelinated mice of susceptible haplotype with functional deficits (51), whereas the axonal transport was preserved in demyelinated β_2m-deficient mice (52). Finally, genetic deletion of perforin, critical mediator of $CD8^+$ T-cells cytotoxic effect, in C57BL/6 H-2^b mice broke viral resistance and resulted in widespread demyelination but conferred protection of motor function along with spinal cord axon numbers (17). Taken together, these observations lend support to the hypothesis that $CD8^+$ T cells injure denuded axons after recognizing axonal MHC class I.

Along with glutamate, N-acetyl aspartate (NAA) is the most abundant free amino acid in nervous tissue (8) with predominantly neuronal localization (26). Because of relatively high concentrations in the brain, NAA provides a prominent peak in the magnetic resonance (MR) spectrum *in vivo*. Therefore, during the last two decades, NAA became attractive for magnetic resonance spectroscopy (MRS) studies in many animal models of neurologic disease. Using TMEV-induced demyelinating disease in two strains of mice with different reparative phenotypes, we used NAA in the mouse brain stem as a surrogate marker of axon injury/preservation throughout the spinal cord (12).

It is evident that $CD8^+$ T cells have an important role in MS lesions and in the development of neurological deficits. Animal models are necessary to further study and elucidate mechanisms by which $CD8^+$ T cells exert deleterious or potentially protective effects (20). The main focus of this manuscript is to determine the role of $CD8^+$ T cells on spinal cord pathology, axonal injury and brainstem NAA levels following TMEV-induced demyelination in two susceptible mouse strains, one of which does not have $CD8^+$ due to β_2m deficiency.

METHODS

Mice

$\beta2m^{+/+}$ mice (Jackson Laboratories, Bar Harbor, ME, USA) were housed and bred in Mayo Clinic's animal care facility. $\beta2m^{-/-}$ mice on resistant H-2^b background were purchased from Jackson Laboratories and then backcrossed eight generations to H-2^q background. The presence of the β2m deletion was confirmed in each generation of the cross by polymerase chain reaction (PCR). After crossing was completed, homozygosity for the Q-haplotype was confirmed by fluorescence-activated cell sorting (FACS). Animal protocols were approved by the Mayo Clinic Institutional Animal Care and Use Committee.

Theiler's virus model of demyelination

Demyelinating disease was induced in 6- to 8-week-old mice by intracerebral injection of TMEV. A 27-gauge needle delivered 10 μL containing 2.0×10^5 plaque-forming units of Daniel's strain of TMEV. This resulted in >98% incidence of infection with rare fatalities.

Spinal cord morphometry

Spinal cord morphometry was assessed in both strains at 21, 45, 90, 180, 270 and 330–390 days postinfection (dpi). Mice were anesthetized with sodium pentobarbital and perfused intracardially with Trump's fixative (phosphate-buffered 4% formaldehyde/1% glutaraldehyde, pH 7.4). Spinal cords were removed and sectioned precisely into 1-mm blocks. In order to represent the samples along the length of the spinal cord, every third block was postfixed, stained with osmium tetroxide and embedded in araldite plastic (Polysciences, Warrington, PA, USA). One-micron sections were cut and stained with 4% *p*-phenylenediamine to visualize the myelin sheaths. Ten spinal cord cross sections, spanning the entire spinal cord from cervical to the distal lumbar spinal column regions, were examined from each mouse. Each quadrant from every coronal section from each mouse was graded for presence of inflammation, demyelination and remyelination. Areas of demyelination are characterized by naked axons, cellular infiltration and macrophages with engulfed myelin debris. Abnormally thin myelin sheaths relative to axonal diameter and absence of Schwann cells are indicative of oligodendrocyte remyelination. Thick myelin sheaths and the one-to-one relationship between axons and Schwann cells identify Schwann cell remyelination. Areas of demyelination and remyelination are well demarcated and allow accurate quantitative assessment at the 10× and 40× magnifications, respectively. The demyelination score was expressed as the percentage of spinal cord quadrants examined with the pathological abnormality. A maximum score of 100 indicated a particular pathological abnormality in every quadrant of all spinal cord sections of a given mouse. A spinal cord quadrant was considered remyelinated if greater than 75% of the axons in the field showed remyelination. Remyelination score was calculated as the ratio (%) of spinal cord quadrants with remyelination as the function of the number of spinal cord quadrants with pathologic white matter abnormalities (demyelination) which had the potential to be remyelinated. All grading was performed on coded sections without the knowledge of the experimental group.

Immunohistochemistry and image analysis

We performed immunocytochemistry to detect astrocytes and microglial cells. For this analysis, we chose three $\beta2m^{+/+}$ mice that showed no remyelination and three $\beta2m^{-/-}$ mice with extensive remyelination, whereas demyelination levels were equivalent. Five blocks from the spinal cord of these mice were embedded in paraffin. We stained for glial fibrillary acidic protein (GFAP, as a marker of astrogliosis) and BS-1 lectin (marker for microglia/macrophages). Immunocytochemical staining was performed

using an ABC Standard Elite kit (Vector Labs, Burlingame, CA, USA). The following primary antibodies were used: GFAP antibody (1:4000, Abcam, Cambridge, MA, USA) and biotinylated *Bandeiraea simplicifolia* BS-1 lectin (1:75, Sigma, St. Louis, MO, USA). The secondary antibody used for GFAP was biotinylated goat anti-rabbit monoclonal antibody (Vector Labs). Quantitative image analysis was performed as previously established and validated by others (33). An Olympus Provis AX70 microscope fitted with a DP70 digital camera and a 40× objective was used to capture four areas from each section. Images were acquired as tagged image format files to retain maximum resolution. We used ImageJ software (National Institutes of Health, Bethesda, MD, USA) to obtain a threshold optical density that discriminated staining from the background. Data were reported as the percentage of labeled area captured (positive pixels) divided by the full area captured (total pixels).

MRS

MRS was performed using a Bruker Avance 300 MHz (7T) vertical bore NMR spectrometer (Bruker Biospin, Billercia, MA, USA) equipped with imaging accessories. During data acquisition, animal core temperature was maintained at 37°C by a flow of warm air. Inhalational isoflurane anesthesia 1.5–2.5% in oxygen was delivered via nose cone. MRS data were obtained from a $(2.5 \times 2.5 \times 2.5)$ mm^3 voxel (15.625 μL), placed over the brain stem as previously reported (12). The same investigator selected all voxels based on anatomical landmarks to maintain strict uniformity throughout the study. Bruker's volume selective sequence, an implementation of the standard PRESS sequence, was used for voxel-based spectroscopy, with built-in water suppression pulses. First time course experiment on $\beta 2m^{+/+}$ animals was performed with repetition time (TR) 2000 ms, echo time (TE) 100 ms, 2048 averages and manual shimming. For $\beta 2m^{-/-}$ animals, the system was upgraded allowing automatic shimming and shorter TE (TE 50 ms). Shorter TR improved the signal to noise; thus, 768 averages were used.

Processing

Collected spectra were analyzed using LCModel (40, 41). The unsuppressed water signal measured from the same voxel was used as an internal reference for quantification (assuming 77% brain water content from our measurements). The LCModel analysis calculates the best fit to the experimental spectrum as a linear combination of model spectra (solution spectra of brain metabolites). Error estimates in metabolite quantification in LCModel are expressed in relative Cramér–Rao lower bounds (CRLB) [percent standard deviation (%SD)] of the estimated concentrations and represent the 95% confidence intervals of the estimated concentration values. In our study, relative CRLB were lower than 10% for estimates for NAA. The LCModel software uses basis spectra of pure metabolites (40). Because both the TR and TE used to acquire LCModel basis set are typically different from TR and TE used *in vivo*, corrections for T_1 and T_2 relaxation times are necessary. Therefore, for absolute NAA quantification, T_1 and T_2 correction factors were calculated and accounted for as previously reported (2). We used the following estimates for T_1 relaxation times: tNAA = 1214 ms, and for T_2 relaxation times: tNAA = 148 ms, calculated as we previously reported (12).

Axon counts

Counting of mid-thoracic (T6) axons was performed at 90, 180 and 270 dpi. To calculate the number of myelinated axons, a one-micron section was cut from the 1-mm block corresponding to the mid-thoracic (T6) spinal cord section from each animal. This level was chosen because it contains both ascending and descending axons with neuronal soma in the brain stem. To ensure an identical intensity of myelin labeling, all spinal cord T6 sections used in the experiment were stained with the same batch of 4% paraphenylenediamine for exactly 20 minutes. An Olympus Provis AX70 microscope fitted with a DP70 digital camera and a 60× oil immersion objective was used to capture six sample areas of normal-appearing white matter containing a relative absence of demyelination from each cross section, according to the previously described sampling scheme (12). The six fields are collected in a clockwise manner around the spinal cord in order to obtain representative samplings of the posterior-lateral, antero-lateral and anterior columns. Images were centered between the gray matter and meningeal surface. Approximately 400 000 μm^2 of white matter was sampled from each mouse. Absolute myelinated axon numbers were calculated as previously reported (17). After collecting six digitized images, image analysis software was used to segment the gray values (145 to 255) corresponding to the axoplasm in each image. The batch algorithm, generated in Matlab (The Mathworks, Narrick, MA, USA), automatically quantified the number and area (μm^2) of each axon from the segmented binary image after regions corresponding to vasculature, cell bodies and longitudinal axons were excluded based on circularity thresholding. Diameters less than 1 μm were excluded to eliminate structures that did not correspond to axons. Data were represented as the absolute number of all axons sampled per mid-thoracic spinal cord section. All numbers were averaged across all animals per group. Total number of axons from the six areas was then divided in three groups as a function of their caliber: 1–3.99 μm^2 (small-caliber axons), 4–10 μm^2 (medium-caliber axons) and >10 μm^2 (large-caliber axons). In addition, large-caliber axons were represented as a relative frequency distribution by dividing the number of these axons with the total number of sampled axons.

Brain pathology

Brain pathology was assessed after the last MRS measurement, at 270 dpi, using our previously described technique (37). Following perfusion with Trump's fixative, we made two coronal cuts in the intact brain at the time of removal from the skull (one section through the optic chiasm and a second section through the infundibulum). As a guide, we used the *Atlas of the Mouse Brain and Spinal Cord* corresponding to sections 220 and 350, page 6 (47). This resulted in three blocks that were then embedded in paraffin. This allowed for systematic analysis of the pathology of the cortex, corpus callosum, hippocampus, brain stem, striatum and cerebellum. Resulting slides were then stained with hematoxylin and eosin. Pathological scores were assigned without knowledge of experimental group to the different areas of the brain. Each

area of the brain was graded on a four-point scale as follows: 0, no pathology; 1, no tissue destruction but only minimal inflammation; 2, early tissue destruction (loss of architecture) and moderate inflammation; 3, definite tissue destruction (demyelination, parenchymal damage, cell death, neurophagia, neuronal vacuolation); and 4, necrosis (complete loss of all tissue elements with associated cellular debris). Meningeal inflammation was assessed and graded as follows: 0, no inflammation; 1, one cell layer of inflammation; 2, two cell layers of inflammation; 3, three cell layers of inflammation; 4, four or more cell layers of inflammation. The area with maximal tissue damage was used for assessment of each brain region. For total brain scores, the scores from each area of the brain were segregated by animal strain and time after infection. The data were expressed as mean ± standard error of the mean.

Statistics

Data were compared by Student's *t*-test if normally distributed or by Mann–Whitney rank sum test if non-normally distributed. More than two groups were compared by analysis of variance. In all analyses, $P < 0.05$ was considered as statistically significant difference.

RESULTS

Spinal cord pathology is alleviated in β2m$^{-/-}$ mice

Because β2m$^{+/+}$ and β2m$^{-/-}$ mice are of the same susceptible H-2^{q} haplotype, infection with TMEV induces spinal cord pathology in both strains. Three weeks following infection, minimal demyelination was evident in both strains (Figure 1A). At 45 and 90 dpi, demyelination was similar in both strains; however, after this period, demyelination progression was different. As compared to 45 and 90 dpi, demyelination in β2m$^{+/+}$ mice worsened at 180, 270 and 330–390 dpi (Figure 1A). Conversely, at 45 dpi, demyelination in β2m-deficient mice reached a peak and did not worsen throughout the chronic phase of the disease (330–390 dpi). Confirming previously published results (5), demyelinating lesions were most frequent in the anterior and lateral columns of the spinal cord.

In strains that repair, like FVB and SWR strains (5), remyelination typically had a late onset in the disease process. Early remyelination was mostly absent. In this study, in β2m$^{+/+}$ strain, remyelination showed much delayed onset (Figure 1B). First clues of remyelination were observed at 270 dpi, and a bit more at 365 dpi. In this strain, remyelination was almost exclusively Schwann cell mediated, with characteristic thick myelin sheaths observed within demyelinated lesions and one-to-one correlation between Schwann cell and remyelinated axon (Supporting Information Figure S1A). However, compared to β2m$^{+/+}$, β2m-deficient mice showed (i) earlier onset of remyelination (at 90 dpi); (ii) increasing percent of remyelinated lesions at chronic stages of the disease (at 180, 270 and 330–390 dpi) (Figure 1B); and (iii) when present, remyelination was more complete (Figure 2E–H). In β2m$^{-/-}$ mice remyelination was both Schwann cell mediated and oligodendrocyte mediated with characteristic thin myelin sheaths (Supporting Information Figure S1B). In oligodendrocyte-mediated remyelination, each oligodendrocyte remyelinated approximately 50–100 axons. Moreover, frequency of remyelination was greater in β2m-deficient mice

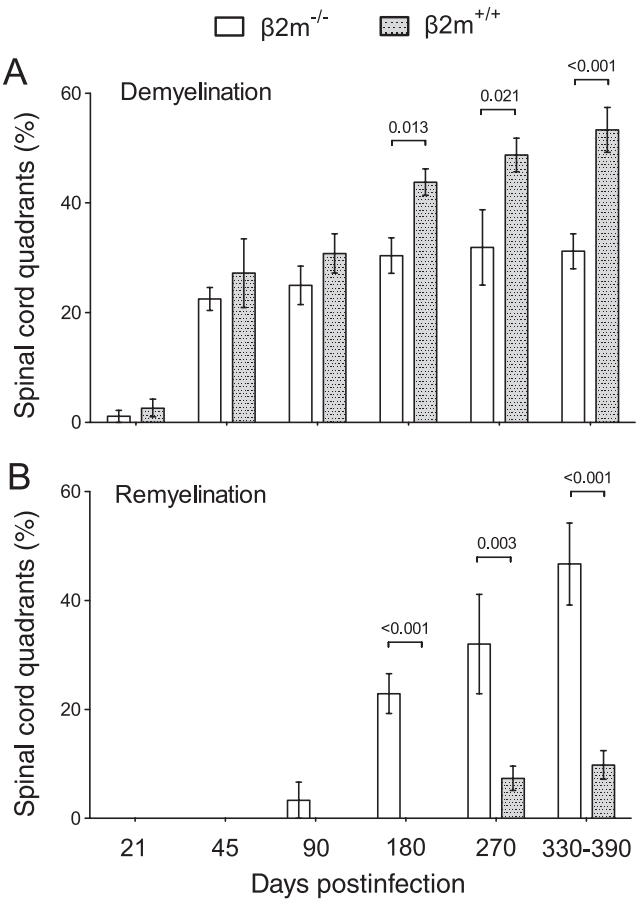

Figure 1. *Spinal cord morphometry in β2m$^{+/+}$ and β2m$^{-/-}$ mice*; **A.** β2m$^{+/+}$ mice are characterized with progressive spinal cord demyelination from 45 dpi and later. At 1 year postinfection, demyelination was prominent in approximately 50% of all analyzed spinal cord quadrants. Conversely, β2m$^{-/-}$ mice had relatively steady levels of demyelination from 45 to 365 dpi. Data expressed as a percentage of quadrants with the demyelination as a function of all spinal cord quadrants examined. **B.** Remyelination in β2m$^{+/+}$ mice was minimal and occurred very late, whereas β2m$^{-/-}$ mice showed remyelination beginning at 90 dpi and was abundant by 270 and 330–390 dpi. Data expressed as a percentage of quadrants with the remyelination as a function of all demyelinated spinal cord quadrants.

(Table 1). Whereas only approximately 50% of β2m$^{+/+}$ mice showed remyelination at 270 and 330–390 dpi, 80–90% of β2m$^{-/-}$ mice remyelinated at 180 through 390 dpi.

Three weeks following infection, β2m$^{-/-}$ mice showed almost fourfold higher levels of meningeal inflammation as compared to β2m$^{+/+}$ mice ($P = 0.003$) (Supporting Information Figure S2A). This was expected because β2m$^{-/-}$ mice do not have CD8^{+} T cells which are critical as the early anti-TMEV response (24). At 45 dpi, inflammation was similar in both strains. However, after 90 dpi, there was a tendency for more inflammation in β2m$^{+/+}$ mice which was in agreement with more demyelination in this strain. Only at 180 dpi, we did not find statistical difference. In addition, at the very late time point when we saw major differences in remyelination, we did not find differences in astrogliosis or activated microglial cells in spinal cord (Supporting Information Figure S2B,C).

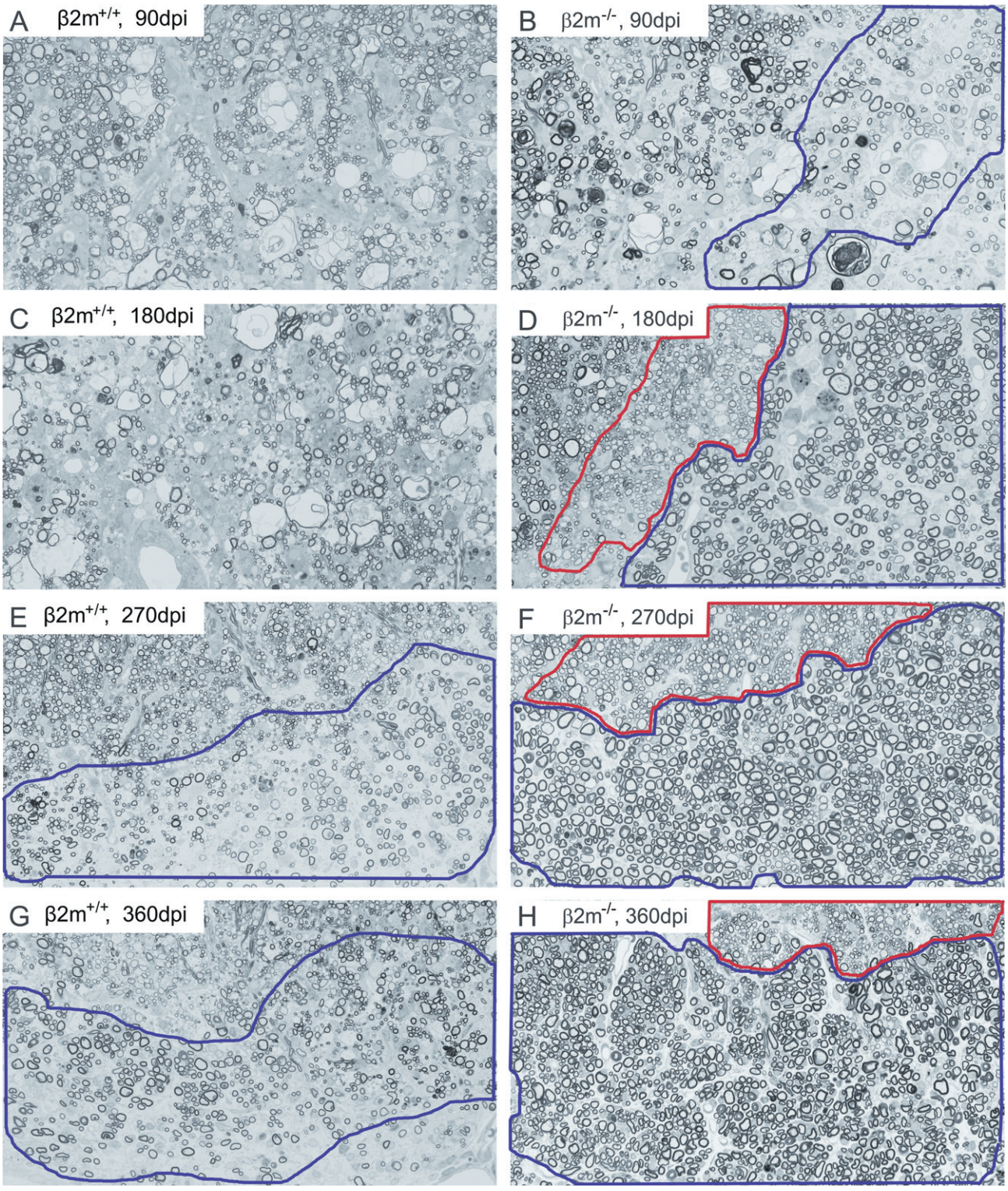

Figure 2. *Remyelination is more extensive in β2m$^{-/-}$ mice than in β2m$^{+/+}$ mice*; **A,B.** Examples of demyelination and no remyelination in both mouse strains. At 90 dpi, only clues of minimal remyelination were observed in several β2m$^{-/-}$ mice. **C,D.** At 180 dpi, remyelination was observed only in β2m$^{-/-}$ mice (**D**). Very late in the disease (270–360 dpi), there were attempts of remyelination in β2m$^{+/+}$ animals (**E,G**), whereas remyelination in β2m$^{-/-}$ mice was extensive and complete (**F,H**). All images were taken from thoracic anterior spinal cord columns, areas with prominent demyelination. Regions that contain Schwann cell remyelination are outlined in blue, whereas regions with oligodendrocyte-mediated remyelination are outlined in red.

Table 1. Spinal cord pathology—frequency of remyelination (n = number of mice).

Days postinfection	β2m$^{+/+}$		β2m$^{-/-}$	
	N	Frequency	N	Frequency
21	15	0%	8	0%
45	6	0%	32	0%
90	18	0%	6	16.7%
180	12	0%	25	80%
270	21	47.6%	7	87.5%
330–390	20	55%	19	89.5%

MRS of the brain stem

We have previously proposed the use of brainstem NAA concentrations as a surrogate marker for spinal cord pathological changes, including demyelination and remyelination (12). Because we observed more remyelination in β2m$^{-/-}$ vs. β2m$^{+/+}$ mice, we compared brainstem NAA levels in these two strains throughout the course of TMEV disease. MRS data were collected from groups of β2m$^{+/+}$ ($n = 10$) and β2m$^{-/-}$ mice ($n = 13$) prior to TMEV infection and prospectively in the same mice at 21, 45, 90, 180 and 270 days after infection. NAA levels in β2m$^{+/+}$ mice significantly decreased at 45 dpi ($P = 0.002$) and remained low throughout the disease course. Significant drop of NAA in β_2m$^{-/-}$ mice occurred at 45 dpi ($P = 0.007$). However, starting with 180 dpi and then at 270 dpi, NAA levels showed recovery (Figure 3). When we compared NAA between two strains, as expected, baseline levels were equivalent.

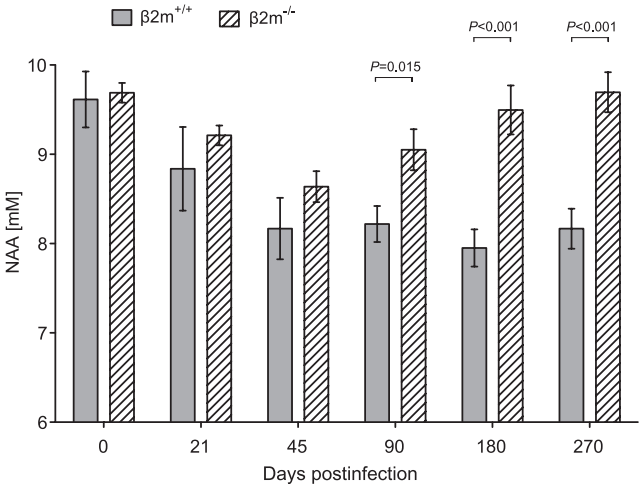

Figure 3. *Longitudinal MRS time course study in β2m$^{+/+}$ and β2m$^{-/-}$ mice.* MRS data were collected from groups of 10–13 β2m$^{+/+}$ and β_2m$^{-/-}$ mice, prior to TMEV infection and repeatedly as disease progressed in the same mice to 270 days postinfection. Bars represent the means of metabolite concentrations of the group with standard error of the mean. NAA levels in both strains were similar in uninfected mice and decreased at 21 and 45 dpi, but from 90 dpi and on NAA levels diverged. Significant differences in NAA concentrations for β2m$^{+/+}$ vs. β_2m$^{-/-}$ mice were observed at day 90 ($P = 0.015$), day 180 ($P < 0.001$) and day 270 ($P < 0.001$).

NAA levels were also similar early in the disease (21 and 45 dpi), but in the chronic stages of the disease, statistically significant differences emerged at 90 dpi ($P = 0.015$), 180 dpi ($P < 0.001$) and 270 dpi ($P < 0.001$) (Figure 3). We additionally scanned 10 2-month-old and six 9-month-old uninfected mice and determined that there were no major changes in NAA levels associated with age.

Brain pathology

To determine whether genetic deletion of β_2m had an impact on the severity of brain pathology, we quantified the pathology in several brains regions from both strains at all time points postinfection. Only very early in the disease (7 dpi), average brain score was significantly higher in β_2m$^{-/-}$ mice ($P = 0.039$, rank sum test) (Figure 4A) as compared to β2m$^{+/+}$ mice. Early brain disease was worse in this strain most probably due to the absence of CD8+ T cells which are most critical for viral clearance from the CNS. At all other time points, postinfection brain pathological scores were equivalent between the strains. After completion of the MRS time course experiment, mice from both strains were sacrificed, and we compared total brain pathology scores and brainstem pathology. No differences in total brain pathology ($P = 0.687$) or brainstem pathology ($P = 0.634$) were observed between β2m$^{+/+}$ and β_2m$^{-/-}$ mice (Figure 4B,C). We concluded that neither total brain pathology nor brainstem pathology was the reason for the observed differences in NAA levels.

Axon counts

Axon counts were performed in both strains of mice used in the MRS time course experiment as well as in uninfected controls, and other mice sacrificed at two time points postinfection (90 dpi and 180 dpi) (Figure 5). We made both intra- and interstrain comparisons. Intrastrain analysis revealed that in β2m$^{+/+}$ mice, there were 5% fewer axons at 90 dpi ($P = 0.2$), 26% fewer at 180 dpi ($P < 0.001$) and 32.8% fewer at 270 dpi compared to uninfected controls ($P < 0.001$). In β_2m$^{-/-}$ mice, at 90 dpi, the number of axons was similar as in normal controls. At 180 dpi, there were 8.5% fewer axons ($P = 0.03$), and, at 270 dpi, there were 15.1% fewer axons ($P < 0.001$) compared to uninfected controls. However, more important was the interstrain comparison. As expected, the number of axons in normal, uninfected mice from both strains was equivalent (Figure 5). At 90 dpi, β2m$^{+/+}$ compared to β2m$^{-/-}$ mice showed a drop in the number of axons which approached statistical significance ($P = 0.057$). Further significant drop in β2m$^{+/+}$ vs. β2m$^{-/-}$ mice was observed at both 180 dpi and 270 dpi ($P < 0.001$). It is important to note that there was some loss of axons even in β2m$^{-/-}$ mice. This implicates that, possibly, CD4+ T cells also contribute to axonal loss but to a lesser extent than CD8+ T cells.

In addition, the total number of axons shown in Figure 5 was divided in three groups as a function of their caliber: 1–3.99 μm^2 (small-caliber axons), 4–10 μm^2 (medium-caliber axons) and >10 μm^2 (large-caliber axons). As disease progresses, β2 m$^{+/+}$ mice showed progressive loss of all caliber axons (Figure 6A). β2 m$^{-/-}$ mice at 90 dpi did not show change in the total number of axons (Figure 5). However, analysis of axon distribution at this time point revealed an interesting finding (Figure 6B). Whereas small-caliber axons were not changed, there was a trend toward redistribution of

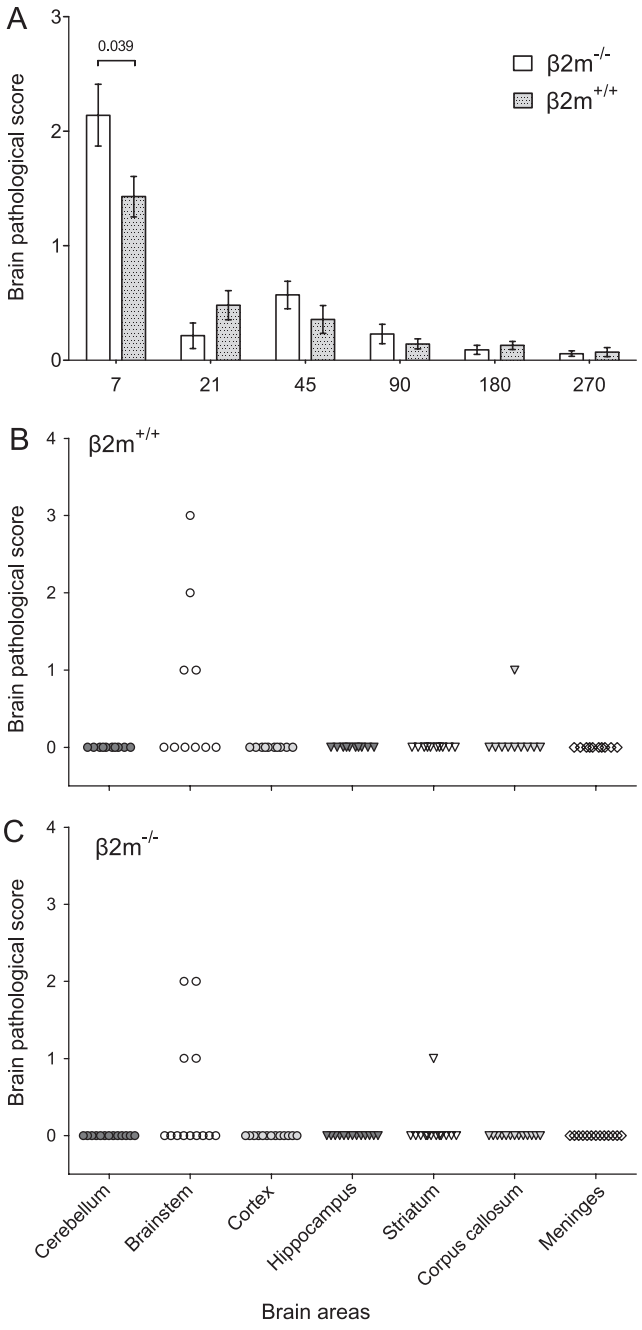

Figure 4. *Brain pathology in infected β2m+/+ and β2m−/− mice*; Seven areas of the brain (cerebellum, brain stem, cortex, hippocampus, striatum, corpus callosum and meninges) were graded independently based on a four-point scale as described in the methodology section. Scores from all areas were averaged and plotted as shown. Bars show the mean ± SEM of each group. **A.** Brain pathology scores in $\beta_2m^{-/-}$ mice compared to β2m+/+ mice showed differences at 7 dpi ($P = 0.039$). At other time points, brain pathology was equivalent. The overall pattern of individual brain pathological scores of β2m+/+ (**B**) and $\beta_2m^{-/-}$ mice (**C**) used in the MR spectroscopy time course study (270 dpi) was similar. We found no significant difference in brainstem pathology scores between the two strains of mice ($P = 0.634$, Mann–Whitney rank sum test).

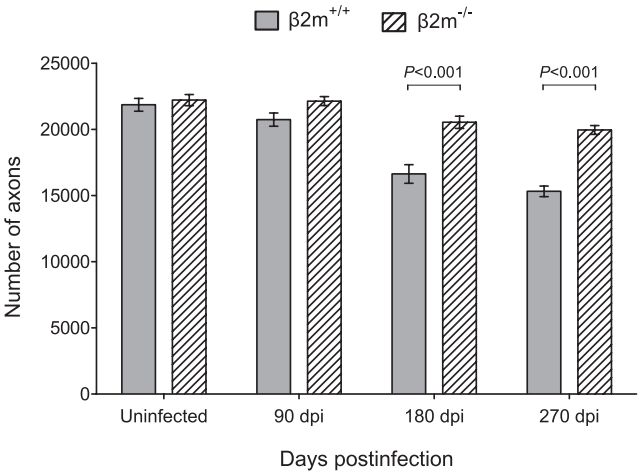

Figure 5. *The total number of myelinated mid-thoracic (T6) axons in uninfected and chronically infected β2m+/+ and β2m−/− mice (interstrain comparison).* The graph shows total number of mid-thoracic axons in uninfected, 90, 180 and 270 dpi β2m+/+ and β2m−/− mice. Bars represent the means of the group with standard error of the mean. Number of axons was not different in uninfected controls from both strains. At 90 dpi, number of axons in β2m+/+ compared to β2m−/− mice decreased and approached statistical significance ($P = 0.057$). At both 180 and 270 dpi, number of axons was significantly lower in β2m+/+ mice ($P < 0.001$).

medium- and large-caliber axons. Compared to uninfected controls, the number of medium-caliber axons increased, whereas the number of large-caliber axons decreased, although the difference was statistically not significant. At 180 dpi, only large-caliber axons showed a statistically significant drop ($P = 0.002$) with a trend toward a decrease in small-caliber axons ($P = 0.061$). However, at 270 dpi, axon loss was significant across all three categories ($P < 0.001$ for small-caliber axons, $P = 0.02$ for medium-caliber axons and $P = 0.002$ for large-caliber axons). The number of large-caliber axons in β2m−/− mice at this chronic time point was reduced by approximately 30% compared to uninfected littermate controls.

Finally, large-caliber axons in both strains at all time points postinfection were represented as a relative frequency distribution by dividing the number of these axons with the total number of sampled axons (Figure 6C). Uninfected controls from both strains had equivalent relative frequencies of large-caliber axons. β2m+/+ mice at 90 dpi and β2m−/− mice at 90, 180 and 270 dpi show equivalent, minimal left and downward shift (axonal loss) in large axons distribution. However, at 180 and even more at 270 dpi, β2m+/+ mice featured the prominent shift of large-caliber axon distributions.

DISCUSSION

There has been increasing evidence regarding the role of CD8+ T cells in several autoimmune and inflammatory CNS diseases, including MS. In TMEV-induced demyelinating disease of mice, CD8+ T cells have dual roles. Resistant strains of mice (H-$2^{b,d,k}$ haplotypes) mount a strong CD8+ T-cell response that clears the

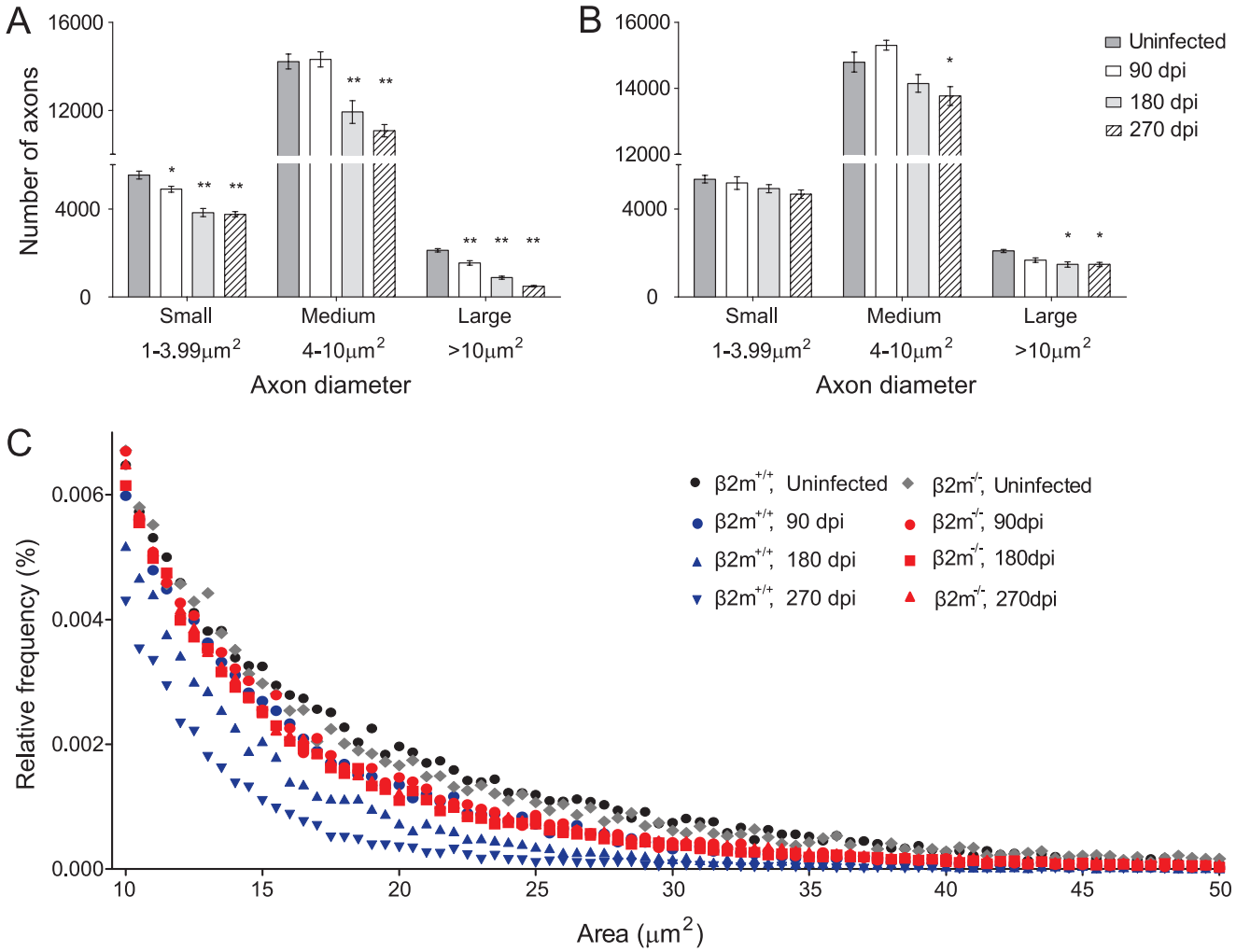

Figure 6. *Mid-thoracic axon distributions in β2m$^{+/+}$ and β2m$^{-/-}$ mice*; **A.** With the progression of disease, β2m$^{+/+}$ mice showed axon loss of all calibers; **B.** At 180 dpi, β2m$^{-/-}$ mice showed statistically significant drop only in large-caliber axons group ($P = 0.002$). At 270 dpi, axon drop was significant across all three categories ($P < 0.001$ for small-caliber axons, $P = 0.02$ for medium-caliber axons and $P = 0.002$ for large-caliber axons). Bars represent the means of the group with standard error of the mean. **C.** Relative frequency distribution of large-caliber axons (>10 μm^2) from both strains at various time points postinfection. The plot shows relative frequencies of large-caliber axons using 0.5 μm^2 intervals as bins. Relative frequencies of large-caliber axons were similar in uninfected controls (black circles and gray triangles). β2m$^{+/+}$ mice at 90 dpi and β2m$^{-/-}$ mice at all time points postinfection showed equivalent minimal left shift in axon distributions (all red symbols and blue circles). Note the prominent left shift of large-caliber axon distributions in β2m$^{+/+}$ mice at 180 (blue triangles) and even more at 270 dpi (blue inverted triangles). Asterisks denote statistically significant difference from the uninfected control (*$P < 0.05$, **$P < 0.001$).

virus from the brain and prevents spinal cord disease (28). In susceptible strains (H-2^{s,v,r,q} haplotypes) during the acute phase of TMEV-induced disease, CD8$^+$ T cells help to clear the virus and infection from the brain but not from the spinal cord (28). Therefore, the role of these cells in the acute phase of the disease is only partially protective. However, during the chronic phase of the disease in susceptible mice, both CD4$^+$ and CD8$^+$ T cells appear to be harmful (10, 11). Still unknown is the antigen in susceptible strains that triggers these cells to become cytotoxic, release cytokines, perforin and granzymes. When spinal cord-infiltrating perforin-competent CD8$^+$ T cells were adoptively transferred into demyelinated but functionally preserved perforin knockout mice, a rapid and irreversible loss of motor function occurred (11). In addition, when CD8$^+$ T cells were immunodepleted in chronically demyelinated mice, motor function was preserved. Taken together, inflammatory tissue damage and development of neurologic deficits in chronic stages of TMEV-induced disease appear to be mediated in part by MHC class I-restricted CD8$^+$ T cells.

It is important to emphasize that the observations of the important role of CD8$^+$ T cells and class I MHC have come from the experiment in the BL (black background) strain of mice (44). One of the most commonly used susceptible strains of mice is SJL/J (of H-2^s haplotype). These mice are of a completely different background and also show a large deletion of T-cell receptor V$_\beta$ genes (4). Of interest, in this strain, CD4$^+$ T cells have a major role in virus-induced demyelination (31, 39), whereas CD8$^+$ T cells have

both damaging and regulatory roles (3). In addition, by studying β2m-deficient SJL mice, Begolka *et al*. showed worsened demyelination, accelerated onset of disease and neurological deficits in this strain (3). Because of these issues, we chose to analyze spinal cord morphometry as well as brainstem MRS in B10.Q $\beta2m^{+/+}$ and $\beta2m^{-/-}$ strains, as genetic analysis in mice of B10 background showed that virus persistence and virus-induced demyelination mapped to H-2D gene of MHC class I (44).

One major finding in this study was that demyelination was worse in $\beta2m^{+/+}$ than in $\beta2m^{-/-}$ mice. Over time, in $\beta2m^{+/+}$ mice, demyelination progressed, but interestingly, in $\beta2m^{-/-}$ mice, demyelination levels were steady from 45 dpi to 390 dpi. In $\beta2m^{+/+}$ mice, remyelination was minimal and occurred at a late onset, whereas in $\beta2m^{-/-}$ mice, remyelination was remarkable and more complete. The most likely explanation for prominent differences in demyelination and remyelination levels was the absence of cytotoxic, axon-damaging $CD8^+$ T cells. However, we can not exclude the possibility that reduced levels of demyelination may partially be due to the absence of $CD8^+$ regulatory T cells. Another possibility is that $CD8^+$ T cells may have had remyelination-inhibiting role (30), which is consistent with the hypothesis that MHC class I is important for the TMEV-induced pathogenesis. Finally, based on our previous experiments, the mechanism of increased demyelination in $\beta2m^{+/+}$ mice is either a result of direct virus infection of oligodendrocytes (43) or as a result of an immune attack to virus antigen (25) or epitope spreading of myelin antigens (31). It is also important to emphasize that $CD8^+$ T cells are not the only culprits of worsened pathology observed in $\beta2m^{+/+}$ mice because demyelination and modest axonal loss were still observed in $\beta2m^{-/-}$ mice. This is in agreement with the previous finding in which both T-cell subsets have discrete contributions to demyelination (34) and possibly also to remyelination.

Analysis by MRS showed that NAA levels in the brain stem decreased in $\beta2m^{+/+}$ mice accordingly with the progression of demyelination, and remained low until the end of the experiment. On the other hand, after a drop at 45 dpi, NAA levels in $\beta2m^{-/-}$ mice recovered at chronic time points as remyelination progressed. The time-associated correlation of brainstem NAA recovery with the remyelination in $\beta2m^{-/-}$ mice strongly agrees with our previous study showing NAA recovery with spontaneous remyelination in FVB mice (12). The findings are consistent with the hypothesis that one of the features of remyelination is the subsequent preservation of axons and their cell bodies in the brain stem. We demonstrated previously that $\beta2m^{-/-}$ mice had increased number of retrograde-labeled brainstem neurons as compared to susceptible mice despite similar levels of demyelination (52). In the current study, we showed that brainstem pathology scores were not different in the two strains used in the MRS time course study. This is consistent with our working hypothesis that spinal cord integrity but not the brainstem pathology influences primarily NAA levels measured by MRS (12).

Counting of mid-thoracic axons at various time points postinfection in $\beta2m^{+/+}$ mice showed extensive axonal loss at chronic time points (180 dpi and 270 dpi). At 270 dpi, this strain lost almost one-third of sampled mid-thoracic axons. In addition, with disease progression, $\beta2m^{+/+}$ mice lost axons of all sizes (small-, medium- and large-caliber axons). Axonal loss in $\beta2m^{-/-}$ mice was also observed in the late phase of the disease (180 dpi and 270 dpi), but was less severe as these mice lost only 15% of sampled mid-thoracic axons. At both of the chronic time points postinfection, there was equivalent (approximately 30%) loss of large-caliber axons which may explain the better preserved motor function in $\beta2m^{-/-}$ mice (52). McGavern *et al*. showed previously that motor activity measured by rotarod assay correlated with the number of large-caliber axons (27). In addition, chronically infected $\beta2m^{-/-}$ mice (270 dpi) showed approximately 25% reduction in motor activity when tested by rotarod assay (52). The observed 30% loss of large-caliber axons in this study is in agreement with those previous findings.

Even though the number of mid-thoracic axons was not greatly reduced at 90 dpi, NAA levels showed a drop in both strains. The possible reason why NAA levels correlated with demyelination and not with the number of axons at 90 dpi may lie in the specific pathophysiology of denuded axons. NAA is primarily located in the mitochondria, organelles that are the site of oxidative processes essential to provide the energy utilized by axons. Two independent studies showed correlation of demyelination with increased number of intra-axonal mitochondria (35, 46). In addition, it was proposed previously that NAA loss may be reversible or irreversible, depending upon the length or extent of the mitochondrial dysfunction (8). Because of a greater demand for energy metabolism in demyelinated axons, there is a redistribution of mitochondria from brainstem cell bodies to their corresponding axons. As a consequence, brainstem NAA levels decrease at this point. Subsequently, if the demyelination persists (like in $\beta2m^{+/+}$ mice), axons will degenerate and NAA loss will be permanent. However, in $\beta2m^{-/-}$ mice, remyelination subsequently occurs; axons are protected which explains recovery of NAA levels at the chronic time points. This is corroborated by the increasing differences in the number of axons between these strains at the chronic time points (180 dpi and 270 dpi). Therefore, the lack of $CD8^+$ T cells in $\beta2m^{-/-}$ mice on susceptible background allows axonal preservation, compensatory redistribution of sodium channels resulting in less neurologic deficits (42). Similarly, there has been a report regarding increased density of sodium channels in demyelinated human MS lesions (32) and an autopsy study of clinically silent and benign MS with profound demyelination (29). Possibly the lack of neurologic difficulties in these patients dying with clinically silent MS may have been the result of less axonal damage by the absence of $CD8^+$ T cells.

The results from this study along with other recent studies (10, 11, 17, 49) provide further support for the hypothesis that $CD8^+$ T cells are the primary mediators of axonal injury and subsequent neurological deficits in both TMEV model and human MS. In addition, we provide support for the concept that $CD8^+$ T cells may also influence the degree of demyelination and/or remyelination. This suggests that therapeutic targeting of cytotoxic $CD8^+$ T cells may ameliorate some of the consequences of chronic demyelination in human MS.

ACKNOWLEDGMENTS

This work was supported by grants from the NIH (R01 GM092993, R01 NS024180, R01 NS032129, R01 NS048357 and R21 NS073684) and the National Multiple Sclerosis Society (CA 1060A11). We also acknowledge with thanks the support from the Applebaum and Hilton Foundations, the Minnesota Partnership Award for Biotechnology and Medical Genomics and the European

Regional Development Fund -Project FNUSA-ICRC (No. CZ.1.05/1.1.00/02.0123). We thank Laurie Zoecklein and Louisa Papke for their technical assistance. The authors also thank Dr. Stephen Provencher, Oakville, Ontario, for generously providing simulated basis sets for LCModel.

REFERENCES

1. Babbe H, Roers A, Waisman A, Lassmann H, Goebels N, Hohlfeld R *et al* (2000) Clonal expansions of CD8(+) T cells dominate the T cell infiltrate in active multiple sclerosis lesions as shown by micromanipulation and single cell polymerase chain reaction. *J Exp Med* **192**:393–404.
2. Baker EH, Basso G, Barker PB, Smith MA, Bonekamp D, Horska A (2008) Regional apparent metabolite concentrations in young adult brain measured by (1)H MR spectroscopy at 3 Tesla. *J Magn Reson Imaging* **27**:489–499.
3. Begolka WS, Haynes LM, Olson JK, Padilla J, Neville KL, Dal Canto M *et al* (2001) CD8-deficient SJL mice display enhanced susceptibility to Theiler's virus infection and increased demyelinating pathology. *J Neurovirol* **7**:409–420.
4. Behlke MA, Chou HS, Huppi K, Loh DY (1986) Murine T-cell receptor mutants with deletions of beta-chain variable region genes. *Proc Natl Acad Sci U S A* **83**:767–771.
5. Bieber AJ, Ure DR, Rodriguez M (2005) Genetically dominant spinal cord repair in a murine model of chronic progressive multiple sclerosis. *J Neuropathol Exp Neurol* **64**:46–57.
6. Bitsch A, Schuchardt J, Bunkowski S, Kuhlmann T, Bruck W (2000) Acute axonal injury in multiple sclerosis. Correlation with demyelination and inflammation. *Brain* **123**:1174–1183.
7. Booss J, Esiri MM, Tourtellotte WW, Mason DY (1983) Immunohistological analysis of T lymphocyte subsets in the central nervous system in chronic progressive multiple sclerosis. *J Neurol Sci* **62**:219–232.
8. Clark JB (1998) N-acetyl aspartate: a marker for neuronal loss or mitochondrial dysfunction. *Dev Neurosci* **20**:271–276.
9. Coles AJ, Compston DA, Selmaj KW, Lake SL, Moran S, Margolin DH *et al* (2008) Alemtuzumab vs. interferon beta-1a in early multiple sclerosis. *N Engl J Med* **359**:1786–1801.
10. Deb C, Lafrance-Corey RG, Zoecklein L, Papke L, Rodriguez M, Howe CL (2009) Demyelinated axons and motor function are protected by genetic deletion of perforin in a mouse model of multiple sclerosis. *J Neuropathol Exp Neurol* **68**:1037–1048.
11. Deb C, Lafrance-Corey RG, Schmalstieg WF, Sauer BM, Wang H, German CL *et al* (2010) CD8+ T cells cause disability and axon loss in a mouse model of multiple sclerosis. *PLoS ONE* **5**:e12478.
12. Denic A, Bieber A, Warrington A, Mishra PK, Macura S, Rodriguez M (2009) Brainstem (1)H nuclear magnetic resonance (NMR) spectroscopy: marker of demyelination and repair in spinal cord. *Ann Neurol* **66**:559–564.
13. Ford ML, Evavold BD (2005) Specificity, magnitude, and kinetics of MOG-specific CD8+ T cell responses during experimental autoimmune encephalomyelitis. *Eur J Immunol* **35**:76–85.
14. Friese MA, Fugger L (2005) Autoreactive CD8+ T cells in multiple sclerosis: a new target for therapy? *Brain* **128**:(Pt 8): 1747–1763.
15. Goverman J, Perchellet A, Huseby ES (2005) The role of CD8(+) T cells in multiple sclerosis and its animal models. *Curr Drug Targets* **4**:239–245.
16. Hauser SL, Bhan AK, Gilles F, Kemp M, Kerr C, Weiner HL (1986) Immunohistochemical analysis of the cellular infiltrate in multiple sclerosis lesions. *Ann Neurol* **19**:578–587.
17. Howe CL, Adelson JD, Rodriguez M (2007) Absence of perforin expression confers axonal protection despite demyelination. *Neurobiol Dis* **25**:354–359.
18. Huseby ES, Liggitt D, Brabb T, Schnabel B, Ohlen C, Goverman J (2001) A pathogenic role for myelin-specific CD8(+) T cells in a model for multiple sclerosis. *J Exp Med* **194**:669–676.
19. Jilek S, Schluep M, Rossetti AO, Guignard L, Le Goff G, Pantaleo G, Du Pasquier RA (2007) CSF enrichment of highly differentiated CD8+ T cells in early multiple sclerosis. *Clin Immunol* **123**:105–113.
20. Johnson AJ, Suidan GL, McDole J, Pirko I (2007) The CD8 T cell in multiple sclerosis: suppressor cell or mediator of neuropathology? *Int Rev Neurobiol* **79**:73–97.
21. Junker A, Ivanidze J, Malotka J, Eiglmeier I, Lassmann H, Wekerle H *et al* (2007) Multiple sclerosis: T-cell receptor expression in distinct brain regions. *Brain* **130**:(Pt 11):2789–2799.
22. Koller BH, Marrack P, Kappler JW, Smithies O (1990) Normal development of mice deficient in beta 2M, MHC class I proteins, and CD8+ T cells. *Science* **248**:1227–1230.
23. Kuhlmann T, Lingfeld G, Bitsch A, Schuchardt J, Bruck W (2002) Acute axonal damage in multiple sclerosis is most extensive in early disease stages and decreases over time. *Brain* **125**:2202–2212.
24. Larsson-Sciard EL, Dethlefs S, Brahic M (1997) In vivo administration of interleukin-2 protects susceptible mice from Theiler's virus persistence. *J Virol* **71**:797–799.
25. Lipton HL, Dal Canto MC (1976) Theiler's virus-induced demyelination: prevention by immunosuppression. *Science* **192**:62–64.
26. Manganas LN, Zhang X, Li Y, Hazel RD, Smith SD, Wagshul ME *et al* (2007) Magnetic resonance spectroscopy identifies neural progenitor cells in the live human brain. *Science* **318**:980–985.
27. McGavern DB, Murray PD, Rivera-Quinones C, Schmelzer JD, Low PA, Rodriguez M (2000) Axonal loss results in spinal cord atrophy, electrophysiological abnormalities and neurological deficits following demyelination in a chronic inflammatory model of multiple sclerosis. *Brain* **123**:(Pt 3):519–531.
28. Mendez-Fernandez YV, Johnson AJ, Rodriguez M, Pease LR (2003) Clearance of Theiler's virus infection depends on the ability to generate a CD8+ T cell response against a single immunodominant viral peptide. *Eur J Immunol* **33**:2501–2510.
29. Mews I, Bergmann M, Bunkowski S, Gullotta F, Bruck W (1998) Oligodendrocyte and axon pathology in clinically silent multiple sclerosis lesions. *Mult Scler* **4**:55–62.
30. Miller DJ, Rivera-Quinones C, Njenga MK, Leibowitz J, Rodriguez M (1995) Spontaneous CNS remyelination in beta 2 microglobulin-deficient mice following virus-induced demyelination. *J Neurosci* **15**:8345–8352.
31. Miller SD, Vanderlugt CL, Begolka WS, Pao W, Yauch RL, Neville KL *et al* (1997) Persistent infection with Theiler's virus leads to CNS autoimmunity via epitope spreading. *Nat Med* **3**:1133–1136.
32. Moll C, Mourre C, Lazdunski M, Ulrich J (1991) Increase of sodium channels in demyelinated lesions of multiple sclerosis. *Brain Res* **556**:311–316.
33. Mori T, Town T, Tan J, Yada N, Horikoshi Y, Yamamoto J *et al* (2006) Arundic acid ameliorates cerebral amyloidosis and gliosis in Alzheimer transgenic mice. *J Pharmacol Exp Ther* **318**:571–578.
34. Murray PD, Pavelko KD, Leibowitz J, Lin X, Rodriguez M (1998) CD4(+) and CD8(+) T cells make discrete contributions to demyelination and neurologic disease in a viral model of multiple sclerosis. *J Virol* **72**:7320–7329.
35. Mutsaers SE, Carroll WM (1998) Focal accumulation of intra-axonal mitochondria in demyelination of the cat optic nerve. *Acta Neuropathol (Berl)* **96**:139–143.

36. Neumann H, Medana IM, Bauer J, Lassmann H (2002) Cytotoxic T lymphocytes in autoimmune and degenerative CNS diseases. *Trends Neurosci* **25**:313–319.
37. Pavelko KD, Howe CL, Drescher KM, Gamez JD, Johnson AJ, Wei T *et al* (2003) Interleukin-6 protects anterior horn neurons from lethal virus-induced injury. *J Neurosci* **23**:481–492.
38. Polman CH, O'Connor PW, Havrdova E, Hutchinson M, Kappos L, Miller DH *et al* (2006) A randomized, placebo-controlled trial of natalizumab for relapsing multiple sclerosis. *N Engl J Med* **354**:899–910.
39. Pope JG, Karpus WJ, VanderLugt C, Miller SD (1996) Flow cytometric and functional analyses of central nervous system-infiltrating cells in SJL/J mice with Theiler's virus-induced demyelinating disease. Evidence for a CD4+ T cell-mediated pathology. *J Immunol* **156**:4050–4058.
40. Provencher SW (1993) Estimation of metabolite concentrations from localized in vivo proton NMR spectra. *Magn Reson Med* **30**:672–679.
41. Provencher SW (2001) Automatic quantitation of localized in vivo 1H spectra with LCModel. *NMR Biomed* **14**:260–264.
42. Rivera-Quinones C, McGavern D, Schmelzer JD, Hunter SF, Low PA, Rodriguez M (1998) Absence of neurological deficits following extensive demyelination in a class I-deficient murine model of multiple sclerosis. *Nat Med* **4**:187–193.
43. Rodriguez M, Leibowitz JL, Lampert PW (1983) Persistent infection of oligodendrocytes in Theiler's virus-induced encephalomyelitis. *Ann Neurol* **13**:426–433.
44. Rodriguez M, Leibowitz J, David CS (1986) Susceptibility to Theiler's virus-induced demyelination. Mapping of the gene within the H-2D region. *J Exp Med* **163**:620–631.
45. Rodriguez M, Dunkel AJ, Thiemann RL, Leibowitz J, Zijlstra M, Jaenisch R (1993) Abrogation of resistance to Theiler's virus-induced demyelination in H-2b mice deficient in beta 2-microglobulin. *J Immunol* **151**:266–276.
46. Sathornsumetee S, McGavern DB, Ure DR, Rodriguez M (2000) Quantitative ultrastructural analysis of a single spinal cord demyelinated lesion predicts total lesion load, axonal loss, and neurological dysfunction in a murine model of multiple sclerosis. *Am J Pathol* **157**:1365–1376.
47. Sidman RL, Angevine JB, Pierce ET (1971) *Atlas of the Mouse Brain and Spinal Cord*. Harvard Univ Press: Cambridge.
48. Skulina C, Schmidt S, Dornmair K, Babbe H, Roers A, Rajewsky K *et al* (2004) Multiple sclerosis: brain-infiltrating CD8+ T cells persist as clonal expansions in the cerebrospinal fluid and blood. *Proc Natl Acad Sci U S A* **101**:2428–2433.
49. Sobottka B, Harrer MD, Ziegler U, Fischer K, Wiendl H, Hunig T *et al* (2009) Collateral bystander damage by myelin-directed CD8+ T cells causes axonal loss. *Am J Pathol* **175**:1160–1166.
50. Sun D, Whitaker JN, Huang Z, Liu D, Coleclough C, Wekerle H, Raine CS (2001) Myelin antigen-specific CD8+ T cells are encephalitogenic and produce severe disease in C57BL/6 mice. *J Immunol* **166**:7579–7587.
51. Ure D, Rodriguez M (2000) Extensive injury of descending neurons demonstrated by retrograde labeling in a virus-induced murine model of chronic inflammatory demyelination. *J Neuropathol Exp Neurol* **59**:664–678.
52. Ure DR, Rodriguez M (2002) Preservation of neurologic function during inflammatory demyelination correlates with axon sparing in a mouse model of multiple sclerosis. *Neuroscience* **111**:399–411.
53. van Oosten BW, Lai M, Hodgkinson S, Barkhof F, Miller DH, Moseley IF *et al* (1997) Treatment of multiple sclerosis with the monoclonal anti-CD4 antibody cM-T412: results of a randomized, double-blind, placebo-controlled, MR-monitored phase II trial. *Neurology* **49**:351–357.

SUPPORTING INFORMATION

Additional Supporting Information may be found in the online version of this article:

Figure S1. Examples of Schwann cell and oligodendrocyte-mediated remyelination; **A.** Schwann cell-mediated remyelination is characterized by thick myelin sheaths around the axons. There is a one to one correlation between remyelinated axons and Schwann cells (red stars). **B.** Oligodendrocyte-mediated remyelination features thin myelin sheath which is distinct from both normal myelin and Schwann cell remyelination.

Figure S2. Levels of spinal cord inflammation, astrogliosis (and activated microglial cells) in $\beta2m^{+/+}$ and $\beta2m^{-/-}$ mice; **A.** Early in the disease (21 dpi), spinal cord inflammation was significantly higher in $\beta2m^{-/-}$ mice ($P = 0.003$). At 45 dpi, inflammation was equivalent ($P = 0.9$). Except at 180 dpi, from 90 dpi and on, $\beta2m^{+/+}$ mice overall had more spinal cord inflammation: day 90 ($P = 0.009$), day 270 ($P = 0.04$) and day 330–390 ($P = 0.013$). **B.** Quantitative image analysis of mid-thoracic spinal cord areas showed that GFAP burden was similar in $\beta2m^{+/+}$ and $\beta2m^{-/-}$ mice at the 270 dpi, time point with the biggest differences in remyelination and NAA levels. **C.** Likewise, at 270 dpi, quantitative image analysis of mid-thoracic spinal cord areas showed that BS-1 lectin burden was similar in $\beta2m^{+/+}$ and $\beta2m^{-/-}$ mice.

Please note: Wiley-Blackwell are not responsible for the content or functionality of any supporting materials supplied by the authors. Any queries (other than missing material) should be directed to the corresponding author for the article.